sustainability

MDPI

Article

Methods for Measuring and Assessing Irregularities of Stone Pavements—Part I

Giuseppe Loprencipe *, Salvatore Bruno, Giuseppe Cantisani, Antonio D'Andrea, Paola Di Mascio and Laura Moretti

Department of Civil, Constructional and Environmental Engineering, Sapienza University of Rome, Via Eudossiana 18, 00184 Rome, Italy

* Correspondence: giuseppe.loprencipe@uniroma1.it; Tel.: +39-0644585112

Abstract: Stone pavements are the historical, architectural, and cultural heritage of lots of cities in Italy and the world. Road managers should be able to make decisions on the global conditions to define the most suitable strategies and maintenance interventions for every type of pavement. There are no standard monitoring methods or criteria for evaluating stone pavement performance. These pavements have more uneven surfaces than traditional pavements, but this characteristic could be accepted if type of vehicles and relative travel conditions are considered. Therefore, it is useful to define criteria for assessing roughness considering the comfort experienced by users in different vehicles. In this research, both traditional and innovative methodologies for assessing irregularities have been investigated using true stone surface profiles. In this regard, traditional performance indicators such as the International Roughness Index (IRI) defined by the ASTM E1926, the ISO 8608 classification, and the frequency-weighted vertical acceleration (a_{wz}) provided by ISO 2631-1 for comfort assessment have been considered. In the case of comfort assessment, three dynamic vehicle models (bike, automobile, and bus) have been adopted. Finally, this two-part paper also proposes an innovative straightedge analysis for stone pavements (SASP) to evaluate the effect on traffic of both pavement profile roughness and localized irregularities. In this way, the authors aim to provide an effective tool to monitor stone pavements.

Keywords: stone pavements; pavement irregularities assessment; whole body vibration; ISO8608; ISO2631; urban road safety; vulnerable road users; user riding comfort

check for updates

Citation: Loprencipe, G.; Bruno, S.; Cantisani, G.; D'Andrea, A.; Di Mascio, P.; Moretti, L. Methods for Measuring and Assessing Irregularities of Stone Pavements—Part I. *Sustainability* **2023**, *15*, 1528. https://doi.org/10.3390/su15021528

Academic Editors: Rosolino Vaiana and Vincenzo Gallelli

Received: 29 November 2022
Revised: 28 December 2022
Accepted: 10 January 2023
Published: 12 January 2023

Copyright: © 2023 by the authors. Licensee MDPI, Basel, Switzerland. This article is an open access article distributed under the terms and conditions of the Creative Commons Attribution (CC BY) license (https://creativecommons.org/licenses/by/4.0/).

1. Introduction

Historic stone pavements are of undisputed aesthetic value and are the architectural and cultural heritage of several cities around the world, but often they lead to management issues in urban road networks [1]. These pavements were not designed to accommodate modern traffic categories. They consist of juxtaposed modular elements of non-flat shapes with interposed joints, and their final configuration is an irregular surface in all wavelengths of the worldwide accepted definition [2], even when the pavement has just been built. In particular, the irregularity of a new stone pavement depends on the pavers' size, the construction technique (flat, concave, bush-hammered surface, etc.), the joints' width and type (open, sealed with mortar, etc.) [3,4], and the bedding layer [5]. Factors negatively affecting the functional performances of these pavements are climate change [6] and motor vehicle traffic. It has to be noted that stone pavements often have more irregularities than traditional asphalt concrete (AC) or cement concrete (CC) ones, and that they may not guarantee acceptable conditions of safety and comfort for vehicles and users [7]. Concerning the safety of vehicles moving on uneven surfaces, it is generally observed that the risk of rollover and skidding increases on uneven pavements [8]. Natural stone pavers can cause unsafe conditions for motorcyclists by reducing the amount of friction (skid resistance) or creating an uneven rolling surface [9]. Indeed, pavement roughness negatively affects the contact between the wheel and the surface [10,11], as confirmed by [12,13].

The functional issues of stone pavements spark debates amongst both expert critics and common public opinion. It is not always possible to find a compromise, and the most frequent interventions are as follows:

- The removal of stone pavements from roads with high traffic volumes and reuse of the stones in low- and light-traffic areas [14];
- The implementation of speed reduction to allow circulation in urban roads of all traffic categories and ensure riding comfort [15].

Whatever the admitted road users, the network manager should guarantee a minimum level of pavement regularity to ensure riding comfort and minimize the impact on the surrounding environment in terms of rolling noise and vibrations compared to traditional pavements [16,17]. Experimental data allow assessing the pavement state of health by adopting one or more indices about structural and/or functional conditions [18]. The comparison between the measured values and consolidated threshold values enables us to assess the current pavement condition and schedule the maintenance program. This decision-making process is part of the Pavement Management System (PMS), which allows for identifying priorities and planning interventions based on collected data and future projections, feasibility analysis, and budget optimization [19].

The identification of the monitoring and evaluation criteria for modular stone pavements in the scientific literature [20] has been marginally addressed. Garilli et al. [21] proposed a method to evaluate the functional and safety characteristics of stone pavements used by pedestrians with wheeled trolleys.

A proper method to assess roughness conditions cannot overlook the operating conditions (e.g., speed) and the users (e.g., pedestrians, two-wheeled vehicles, vehicles, buses). Road pavement roughness is a pivotal functional requirement adopted by road managers as a key performance indicator (KPI) to plan maintenance [22]. The International Roughness Index (IRI) is nowadays accepted for both AC and CC carriageways [23]. Accurate IRI decay curves allow road managers to plan network maintenance that optimizes the available resources [24]. Several studies have been proposed to define appropriate IRI thresholds concerning different operational and functional requirements such as the length of the road section [23,25,26], the effects on dynamic loads [27], comfort [28], or the contribution of the joints [4]. Other researchers have investigated the relationship between IRI and the comfort experienced on-board different types of vehicles [29–31] whilst also considering the operating speeds of the road [32]. All these studies have demonstrated the versatility of this index in evaluating the condition of paved surfaces. However, there is a limitation concerning the operating speed and the types of assessed distress. In regard to speed, different thresholds have been proposed as a function of the operating speed [33–35]. These studies have shown that while the threshold values provided by road agencies refer to travel speeds above 80 km/h, higher IRI values can be generally accepted on roads travelled at lower speeds. Moreover, while the evaluation through the IRI is ideal for widespread defects, it performs poorly in interpreting isolated and localized defects [36]. In this regard, an alternative approach has been proposed to evaluate the longitudinal roughness through users' perception [37].

Another interesting approach to evaluating pavement roughness is the Power Spectral Density (PSD) of the profiles according to ISO 8608 [38]. Several studies have adopted this procedure, which simulates the response of the vehicle suspension system to generate artificial profiles and simulates the behavior of vehicles on uneven pavements [39]. In the field of vehicle design, surface profile classification according to [9] has been adopted to generate artificial road profiles that simulate different conditions to optimize the mechanical components or to verify the suspension parameters of vehicles [40–42]. Other scholars have realized artificial road profiles with given IRI values [43–45].

Smartphone apps or low-cost Inertial Measurement Unit (IMU) systems are modern alternative systems for evaluating pavement conditions in urban areas where driving speed is generally low, localized distresses are widespread, and different types of vehicles move at different speeds. Several applications for smartphones [46] and validated IMU systems [47]

allow the measuring of accelerations on-board a vehicle moving at a fixed speed using as a reference the comfort evaluation parameters provided by the international standard ISO 2631-1 [48]. According to the reference standard, the time history of vertical accelerations calculated with a mechanical model of a vehicle moving on a pavement profile allows the calculation of the frequency-weighted vertical acceleration (a_{wz}).

Finally, the authors proposed a Straightedge Analysis for Stone Pavements (SASP). This derives from the Procedures for Measuring Airfield Pavement Roughness defined by the Federal Aviation Administration (FAA) [49] to obtain the Boeing Bump Index (BBI).

Whatever the adopted method, it is necessary to give straightforward and widely accepted definitions of both surface defects and threshold values. Based on true stone surface profiles, this paper takes into account existing methodologies and proposes a new methodology to evaluate the irregularity conditions of stone pavements. Firstly, the IRI [50] and ISO 8608 standards [38] have been adopted to characterize the pavement roughness. Then, the whole vertical body vibration using three mechanical models (i.e., a bicycle, an automobile, and a bus) at different running speeds has been considered. Therefore, according to [50], it was possible to classify the surveyed pavements in terms of performance classes. Finally, SASP classified the irregularities of the stone pavements and overcame the limitations of the traditional methods.

2. Materials and Methods

2.1. International Roughness Index

IRI derives from studies in the 1980s [51] involving controlled measurements of road surface roughness for 320 m-long road sections under a variety of conditions and by a variety of instruments and methods [52]. It is based on a mathematical model called quarter-car and was developed to assess not only the ride quality on road pavements but also other detrimental effects (e.g., dynamic load increment on both vehicle and pavement) due to the presence of irregularities on the road surfaces. Equation (1) allows IRI calculation according to [50]:

$$IRI = \frac{1}{l}\int_0^{l/v} \left|\dot{z}_s - \dot{z}_u\right| dt \quad (1)$$

where l is the length of the profile in km, v is the simulated speed equal to 80 km/h, $\dot{z}_s$ is the time derivative of vertical displacement of the sprung mass in m, and $\dot{z}_u$ is the time derivative of vertical displacement of the unsprung mass in m. IRI is expressed in slope units (e.g., m/km or mm/m).

Over the world, different threshold values for roughness are prescribed in terms of IRI values for pavement quality control, monitoring, maintenance, and repair planning. According to [23], there is a high heterogeneity of adopted IRI thresholds that depend on road surface type (i.e., asphalt or cement concrete pavements), road functional category, average annual daily traffic (AADT), legal speed limit, segment length considered for its calculation, as well as other variables. Among these, the most important are the maximum driving velocity allowed on the road and the type of vehicle adopted to assess riding comfort. In recent years, some authors have proposed that speed-related IRI thresholds be used for the evaluation of ride quality. In particular, Cantisani and Loprencipe [33] considered an assorted sample of 320 m-long 124 profiles of AC pavements (average IRI = 2.11 m/km; maximum IRI = 5.98 m/km, minimum IRI = 0.55 m/km, and standard deviation of IRI = 1.18 m/km) and defined four ride quality levels (Table 1). For each level, the IRI thresholds depended on the a_{wz} calculated for measured speed values ranging between 30 and 90 km/h.

Table 1. IRI thresholds at different speeds [33].

Ride Quality Level	IRI Thresholds at Different Measured Speeds (m/km)						
	30 km/h	40 km/h	50 km/h	60 km/h	70 km/h	80 km/h	90 km/h
Very Good	<4.17	<3.41	<2.98	<1.87	<1.60	<1.42	<1.15
Good/Fair	4.17–8.34	3.41–6.83	2.98–5.95	1.87–3.73	1.60–3.20	1.42–2.84	1.15–2.31
Mediocre	8.34–11.92	6.83–9.75	5.95–8.51	3.73–5.33	3.20–4.58	2.84–4.06	2.31–3.30
Poor	>11.92	>9.75	>8.51	>5.33	>4.58	>4.06	>3.30

The proposed thresholds are valid for the investigated IRI values and AC pavements. An in-depth study is necessary to apply them to stone pavements, whose IRI values and distribution differ from those investigated by [33]. Indeed, higher IRI values and greater IRI variability are to be expected due to the used dynamic model. Figure 1 shows the response of the IRI quarter car filter to different wavelengths varying the speed vehicle. The red curve represents the transfer function between road excitation and the suspension relative velocity, H_{Vrel}, for the reference quarter-car model with parameters defined for IRI estimation (velocity = 80 km/h). In the same graph, the transfer function H_{Vrel} for velocity = 40 km/h is represented [46] to compare the effect of speed on pavement roughness evaluation. Both curves in Figure 1 have the same diagram shape, but the wavelengths influencing the IRI shorten, decreasing the simulation speed.

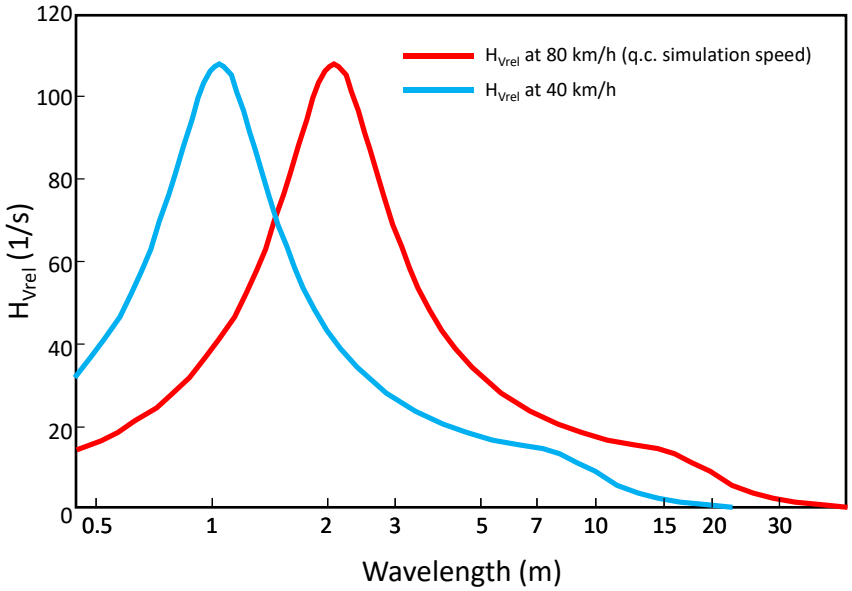

Figure 1. Response of the IRI quarter car filter to different wavelengths.

It cannot be overlooked that the profile length to assess IRI is 320 m. In the urban environment, it is very difficult to collect such a profile length, and shorter sections must be considered. The IRI thresholds on different pavements should refer to the same profile lengths.

For stone pavements, it is difficult to define irregularities threshold values as these pavements have higher values than traditional pavements and an unambiguous definition of surface defects. An attempt to define some threshold values was developed by Zoccali et al. [20] for the so-called Sampietrini, a particular type of stone paving used throughout central Italy and made of stone elements of average dimensions 10 × 10 × 17 cm laid on a 5–10 cm-thick sand bed. For such pavements, Zoccali et al. [20] demonstrated that IRI values were comparable to those obtained for rough unpaved roads (Figure 2). Therefore, IRI values can describe the perceived riding comfort for different speed values, and IRI values more than 8 m/km (dotted red line in Figure 2) imply less than 70 km/h riding speed.

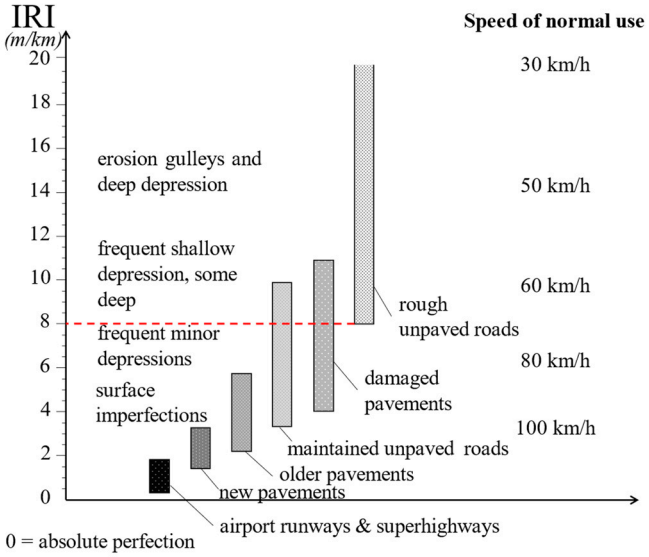

Figure 2. IRI ranges represented by different classes of road.

2.2. Road Surface Profile Classification According to ISO 8608 Standard

Road surface profile classification according to ISO 8608 standard is based on the PSD of the profile. To determine the PSD, it is necessary to measure the surface profile concerning a reference plane [53]. In particular, the Power Spectral Density is calculated using the Fast Fourier Transform (FFT), windowing each profile signal with the Hanning window [54] and representing the smoothed power spectral density. Finally, Equation (2) allows the calculation of the fitted PSD:

$$G_d(n) = G_d(n_0)\left(\frac{n}{n_0}\right)^{-w} \quad (2)$$

where $G_d(n)$ is the fitted PSD [m^3], n is the spatial frequency in cycles/m, $n_0 = 0.1$ cycles/m is the reference spatial frequency, and w is the exponent of the fitted PSD, also known as waviness.

As specified by Múčka and Granlund [55], the two parameters defining $Gd(n)$ (i.e., $G_d(n_0)$ and w) are independent; in particular, the second one provides information about wavelength distribution in the investigated spatial frequency range. Values of waviness greater than two mean that long wavelengths are prevalent, while if w is lower than two, the short ones are predominant.

Based on the $G_d(n_0)$ values, a pavement profile is catalogued according to the classes (from A to H; i.e., from best to worst) defined by [38] (Table 2). Usually, road profiles of AC pavements do not belong to classes worse than D because road agencies set intervention thresholds to restore optimal conditions.

Table 2. ISO 8608 thresholds limits for the road profiles classes.

ISO 8608 Class	$G_d(n_0)$ (10^{-6} m^3)
A	<32
B	32–128
C	128–512
D	512–2048
E	2048–8192
F	8192–32,768
G	32,768–131,072
H	>131,072

Destroyed roads belong to classes above D. However, artificial class profiles higher than D have been generated in the literature [56]. They imply severe distress conditions expected for

unpaved roads. Therefore, the classification proposed by [38] provides a synthetic description of the geometric features of a road pavement surface. However, it overlooks the vehicle type and the driving velocity, and does not properly consider the different vibration levels affecting road users. At any rate, it seems appropriate to use this evaluation method for stone pavements that are characterized by a high level of irregularities.

2.3. Whole-Body Vibration Using Vehicle Mechanical Model Simulation

The international standard ISO 2631-1 allows comfort assessment in public transport [48]. It is based on the analysis of the time-histories of vertical accelerations obtained from direct measurements inside the riding vehicle or simulated by a vehicle mechanical calibrated model. The seat-acceleration time-histories ($a_s(t)$) are processed to determine the vertical Root Mean Square accelerations (a_{iz}^{RMS}) for the ith one-third-octave bands that represent the frequency range of interest for human response to vibrations (i.e., 0.5–80 Hz) according to [48]. Given a_{iz}^{RMS}, Equation (3) allows calculation of the vertical weighted Root Mean Square acceleration (a_{wz}):

$$a_{wz} = \sqrt{\sum_{i=1}^{23} \left(W_{k,i} \cdot a_{iz}^{RMS}\right)^2} \quad (3)$$

where $W_{k,i}$ are the frequency weightings in one-third-octave bands for seated positions provided by [48]; $i = 1, \ldots, 23$.

The a_{wz} values can be compared to the threshold values proposed by [48] (Table 3) to identify the comfort level perceived by road users. The current standard provides several comfort levels and introduces overlapping zones between two adjacent levels because several factors (e.g., user age, acoustic noise, temperature, etc.) contribute to the level of perceived discomfort.

Table 3. a_{wz} threshold values for public transport [47].

a_{wz} Values (m/s^2)	Comfort Level
<0.315	Not uncomfortable
0.315–0.63	Little uncomfortable
0.5–1.0	Fairly uncomfortable
0.8–1.6	Uncomfortable
1.25–2.5	Very uncomfortable
>2.0	Extremely uncomfortable

Innovative Vehicle Mechanical Model Simulation

In this paper, three different dynamic vehicle models have been considered to quantify users' comfort level according to [48]:

- A 5-degree-of-freedom (5-dof) bike model developed in this research and calibrated using parameters proposed by [57–63] to represent the vibration perception of a common biker;
- An 8-dof full-car model developed and calibrated by Cantisani and Loprencipe [33] to represent the vibration perception of a common passenger car (automobile);
- An 8-dof full-car model developed by the authors and calibrated using parameters proposed by [28,64,65] to represent the vibration perception of a common passenger bus;

For each model, the main assumptions are as follows:

- Vehicle body parts are rigidly connected;
- The vehicles move in a straight line, and the longitudinal and transversal variations are assigned by the measured profiles;
- Passenger mass and unsprung mass are considered constant in magnitude during the simulation;
- The input road profiles are responsible for vibration transfer in the vehicle models.

By using Newton's law, Equation (4) is valid for the three vehicle mathematical models:

$$[M]\{\ddot{Z}\} + [\Gamma]\{\dot{Z}\} + [K]\{Z\} = [F] \tag{4}$$

where $[M]$, $[\Gamma]$, $[K]$, and $[F]$ are mass, damping coefficient, spring stiffness, and force matrices, respectively. For example, for the 5-dof bike model in Figure 3, $[M]$, $[\Gamma]$, $[K]$, and $[F]$ are Equations (5)–(8), respectively. Table 4 lists the meaning and the values of the constants and variables.

$$[M] = \begin{bmatrix} m_s & 0 & 0 & 0 & 0 \\ 0 & m & 0 & 0 & 0 \\ 0 & 0 & J_\theta & 0 & 0 \\ 0 & 0 & 0 & m_1 & 0 \\ 0 & 0 & 0 & 0 & m_2 \end{bmatrix} \tag{5}$$

$$[\Gamma] = \begin{bmatrix} c_s & -c_s & r \cdot c_s & 0 & 0 \\ -c_s & c_s + c_1 + c_2 & a_2 \cdot c_2 - a_1 \cdot c_1 - r \cdot c_s & -c_1 & -c_2 \\ r \cdot c_s & a_2 \cdot c_2 - a_1 \cdot c_1 - r \cdot c_s & c_1 \cdot a_1^2 + c_2 \cdot a_2^2 + c_s \cdot r^2 & a_1 \cdot c_1 & -a_2 \cdot c_2 \\ 0 & -c_1 & a_1 \cdot c_1 & c_1 & 0 \\ 0 & -c_2 & -a_2 \cdot c_2 & 0 & c_2 \end{bmatrix} \tag{6}$$

$$[K] = \begin{bmatrix} k_s & -k_s & r \cdot k_s & 0 & 0 \\ -k_s & k_s + k_1 + k_2 & a_2 \cdot k_2 - a_1 \cdot k_1 - r \cdot k_s & -k_1 & -k_2 \\ r \cdot k_s & a_2 \cdot k_2 - a_1 \cdot k_1 - r \cdot k_s & k_1 \cdot a_1^2 + k_2 \cdot a_2^2 + k_s \cdot r^2 & a_1 \cdot k_1 & -a_2 \cdot k_2 \\ 0 & -k_1 & a_1 \cdot k_1 & k_1 + k_{t1} & 0 \\ 0 & -k_2 & -a_2 \cdot k_2 & 0 & k_2 + k_{t2} \end{bmatrix}. \tag{7}$$

$$[F] = \begin{bmatrix} 0 & 0 \\ 0 & 0 \\ 0 & 0 \\ k_{t1} & 0 \\ 0 & k_{t2} \end{bmatrix} \tag{8}$$

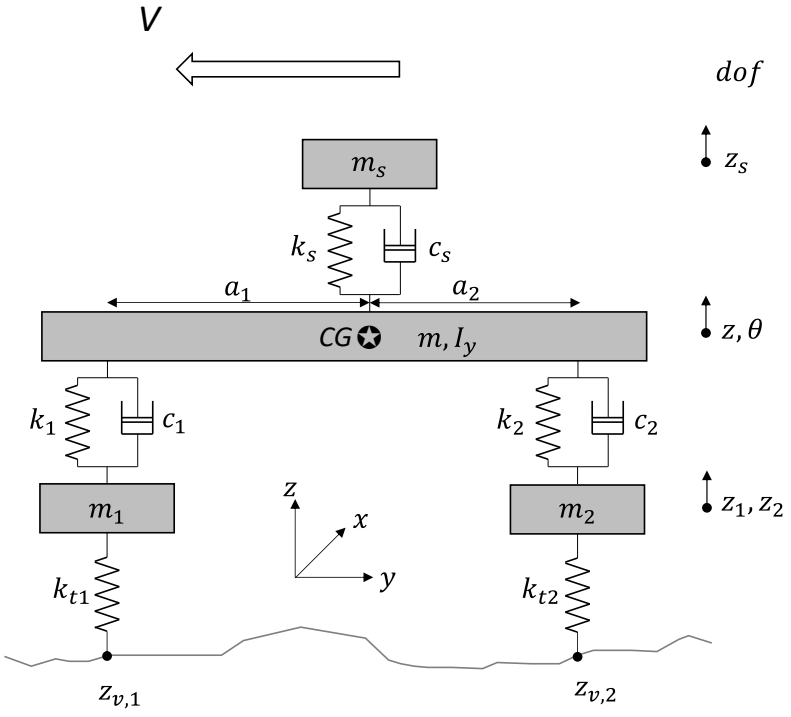

Figure 3. 5-dof mechanical bike model.

Table 4. Constants and variables adopted in the bike 5-dof mathematical model.

Symbol	Value	Unit	Description
m_s	80	kg	Driver body mass
M	20	kg	Bike frame mass without wheels
m_1	2	kg	Mass of a front unsprung mass (wheel)
m_2	2	kg	Mass of a rear unsprung mass (wheel)
J_θ	13	kg m^2	Body (bike) sprung mass pitch moment of inertia
R	0.0	m	Distance of CG from the seat driver
a_1	0.6	m	Distance of CG from the front axle
a_2	0.4	m	Distance of CG from the rear axle
k_1	30,000	N/m	Spring constant suspension front
k_2	25,000	N/m	Spring constant suspension rear
k_{t1}	25,000	N/m	Spring constant tire front
k_{t2}	25,000	N/m	Spring constant tire rear
k_s	50,000	N/m	Spring constant seat driver
c_1	9000	N s/m	Damping constant suspension front
c_2	9000	N s/m	Damping constant suspension rear
c_s	1000	N s/m	Damping constant suspension seat driver
Z	var	m	Body vertical motion coordinate (1-dof)
z_1	var	m	Front-wheel vertical motion coordinate (2-dof)
z_2	var	m	Rear wheel vertical motion coordinate (3-dof)
z_s	var	m	Driver vertical motion coordinate (4-dof)
θ	var	rad	Body pitch motion coordinate (5-dof)
$z_{v,1}$	var	m	Road profile elevation–front
$z_{v,2}$	var	m	Road profile elevation–rear

The differential equations have been implemented in MATLAB® using the State Space representation that describes the set of all possible states of the system [66]. Each coordinate is a state variable whose values completely describe the state of the system [67].

In continuous-time, a state-space model has the following form Equations (9) and (10):

$$\begin{aligned} \dot{z} &= Az + Bu \\ f &= Cz + Du \end{aligned} \tag{9}$$

where

$$[A] = \begin{bmatrix} [Z_{5x5}] & [I_{5x5}] \\ \left[-\frac{M}{K}\right] & \left[-\frac{M}{C}\right] \end{bmatrix} \quad [B] = \begin{bmatrix} [Z_{5x2}] \\ [M/F] \end{bmatrix} \quad [C] = [[I_{10x10}]] \quad [D] = [[Z_{10x2}]] \tag{10}$$

The matrix $[Z(t)]$ Equation (11) contains the discrete time-history of all the parameters to calculate the system dynamic of model:

$$[Z(t)] = \begin{bmatrix} z_s(t) \\ z(t) \\ \theta(t) \\ z_1(t) \\ z_2(t) \\ \dot{z_s}(t) \\ \dot{z}(t) \\ \dot{\theta}(t) \\ \dot{z_1}(t) \\ \dot{z_2}(t) \end{bmatrix} \tag{11}$$

where $z_s(t)$ is the seat vertical motion coordinate in m, $z(t)$ is the body vertical motion coordinate in m, $\theta(t)$ is the body pitch motion coordinate in rad, $z_1(t)$ is the front wheel vertical motion coordinate in m, $z_2(t)$ is the rear wheel vertical motion coordinate in m, $\dot{z_s}(t)$ is the derivate seat vertical motion in m/s, $\dot{z}(t)$ is the derivate body vertical motion

in m/s, $\dot{\theta}(t)$ is the derivate body pitch motion in rad/s, $\dot{z_1}(t)$ is the derivate front wheel vertical motion in m/s, and $\dot{z_2}(t)$ is the derivate rear wheel vertical motion in m/s.

Finally, Equation (12) gives the acceleration time-history of the bike driver:

$$a_s(t) = \frac{k_s \cdot [z(t) - z_s(t)] + c_s \cdot [\dot{z}(t) - \dot{z_s}(t)] + k_s \cdot r \cdot \theta(t) + c_s \cdot r \cdot \dot{\theta}(t)}{m_s} \quad (12)$$

Similarly, the MATLAB® State Space formulation was used to simulate the dynamics of the automobile and the bus using the adopted full-car models. Appendix A lists the matrices and all the geometric and mechanical parameters of the adopted models to assess a_{wz}.

The flow chart in Figure 4 shows the MATLAB® code that carried out the simulations. For each pavement profile, six a_{wz} values were obtained (two driving speed values for each of the three modelled vehicles). Data relating to driving speed and the parameters of the model can be modified, but only those adopted in this study are herein reported.

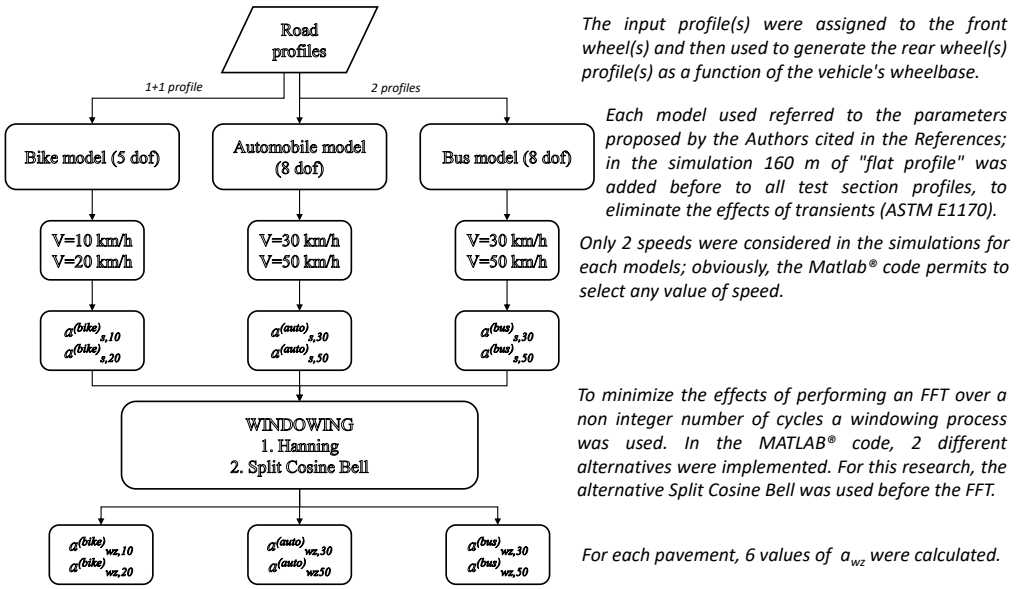

Figure 4. Flow chart of the MATLAB® code implemented for calculating a_{wz}.

In the case of the comfort assessment, the modelled vehicle and the driving speed played a pivotal role in calculating the vertical accelerations perceived by users because they affected the transfer function of the pavement irregularities. In this respect, the contribution of the punctual defects of the pavement cannot be overlooked in a proper evaluation of the examined road section.

2.4. Straightedge Analysis for Stone Pavements

All the methods described in the previous sections allow for a global evaluation of pavement branches for which one or more profiles are known, but when they are used to evaluate the stone paving they have some limits that should be known. In the discussed methods, the results can be influenced by the length of the pavement profile, and it is not possible to identify the contribution of localized geometric defects unless sections of pavement of limited length are cut (however, it is not advisable to go below 20 m). Furthermore, IRI values depend on the position where the localized irregularity occurs (i.e., potholes or bumps, if at the beginning or the end of the profile).

In the case of the comfort assessment, the vehicle used to calculate the vertical acceleration bearing by the user plays a fundamental role for its physical-geometric characteristics and the driving speed as these parameters determine the transfer function of the pavement irregularities. This method also gives a global evaluation of the examined section, and, with difficulty, it is possible to identify the contribution of the punctual defects of the pavement.

For stone pavements, it is necessary to overcome the discussed issues with a method capable of evaluating the effects of localized irregularities. Therefore, this study proposes an innovative approach derived from [49] to identify the position of the most severe irregularities that must be restored. The proposed method is based on the geometric analysis of the true profile of the road collected by profilometric instruments in contact or by 3D surface surveys [64] that allow the extraction of profiles with adequate resolution. The global evaluation of stone pavements consists of the measurement of Bump Heights (BHs) using different theoretical lengths of straightedge (SL_i) that connect two generic points of the L-long profile. The measurement of the BH is carried out for all the possible straightedges, whose lengths range between the minimum value SL_{min} ($SL_{min} = 2{\cdot}\Delta x$) and the maximum one ($SL_{max}$), with step Δx. Equation (13) gives the total number of SL_i (N_{SL}):

$$N_{SL} = \frac{SL_{max} - SL_{min}}{\Delta x} + 1 \tag{13}$$

For example, if Δx = 0.25 m and SL_{max} = 3 m a total of 11 N_{SL} should be considered. Therefore, a true profile can be reduced to $\frac{L}{\Delta x} + 1$ points (X_j, Y_j) where $j = 1, 2, \ldots, \frac{L}{\Delta x} + 1$. For each profile point the straightedge should be positioned to link two points (e.g., X_s, Y_s and X_t, Y_t such that $t > s$).Therefore, for each X_j with $s \leq j \leq t$, the Bump Height is the difference between Y_j and the corresponding straightedge elevation in X_j. Each BH value can be associated to a Bump Length (BL) that is the distance between the X_j point where the BH occurs and the closest of the straightedge extremes. It has to be noted that BL ranges between the minimum value (BL_{min}) equal to Δx and the maximum value (BL_{max}) equal to $SL_{max}/2$. This analysis should be implemented for all the defined SL_i. For example, Figure 5 represents a true road profile (black line) investigated with Δx = 0.25 m, and different straightedges (dotted red lines) whose lengths are d = 1.5 m; m = 2 m; n = 0.75 m, o =1 m; p = 0.5 m; q = 0.5 m; r = 0.5 m.

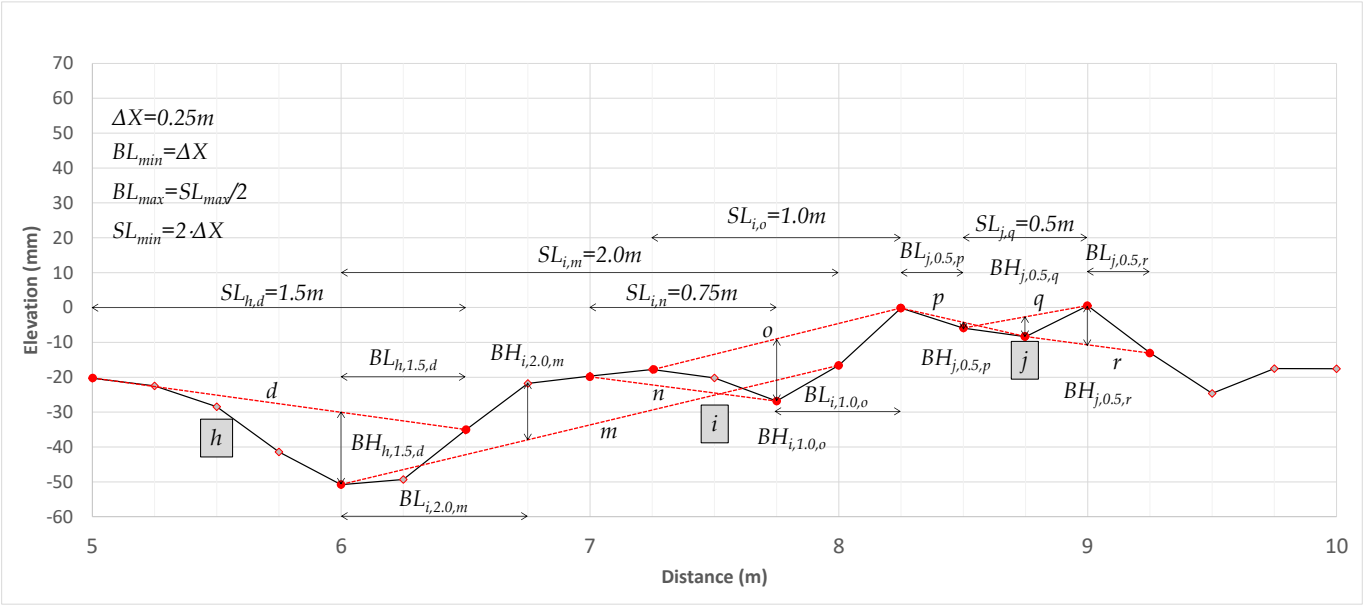

Figure 5. Example of BL, BH and SL in a true pavement profile.

For each point (X_j, Y_j), pairs of BL and BH values are identified; values equal to 0 refer to non-measurable points (Figure 6). For each BL_k (with $k = 1, \ldots, N_{SL} + 1/2$), the maximum and average BH values are calculated as BH_{max} and BH_{avg}, respectively.

			1	2	…	k-1	k	k+1	…	N-1	$N=(N_{SL}+1)/2$
			$1 \cdot \Delta x$	$2 \cdot \Delta x$	…	$(k-1) \cdot \Delta x$	$k \cdot \Delta x$	$(k+1) \cdot \Delta x$	…	$(N-1) \cdot \Delta x$	$N \cdot \Delta x$
			BL_1	BL_2	…	BL_{k-1}	BL_k	BL_{k+1}	…	BL_{N-1}	BL_N
1	0	Y_1	0	0	0	0	0	0	0	0	0
2	$1 \cdot \Delta x$	Y_2	$BH_{1,1}$	0	0	0	0	0	0	0	0
…	…	…	…	…	…	…	…	…	…	…	…
j-1	$(j-2) \cdot \Delta x$	Y_{j-1}	$BH_{j-1,1}$	$BH_{j-1,2}$	…	$BH_{j-1,k-1}$	$BH_{j-1,k}$	$BH_{j-1,k+1}$	…	$BH_{j-1,N-1}$	$BH_{j-1,N}$
j	$(j-1) \cdot \Delta x$	Y_j	$BH_{j,1}$	$BH_{j,2}$	…	$BH_{j,k-1}$	$BH_{j,k}$	$BH_{j,k+1}$	…	$BH_{j,N-1}$	$BH_{j,N}$
j+1	$j \cdot \Delta x$	Y_{j+1}	$BH_{j+1,1}$	$BH_{j+1,2}$	…	$BH_{j+1,k-1}$	$BH_{j+1,k}$	$BH_{j+1,k+1}$	…	$BH_{j+1,N-1}$	$BH_{j+1,N}$
…	…	…	…	…	…	…	…	…	…	…	…
M-1	$(M-2) \cdot \Delta x$	Y_{M-1}	$BH_{M-1,1}$	0	0	0	0	0	0	0	0
$M=L/\Delta x+1$	$(M-1) \cdot \Delta x$	Y_M	0	0	0	0	0	0	0	0	0
			$BH_{max,1}$	$BH_{max,2}$	…	$BH_{max,k-1}$	$BH_{max,k}$	$BH_{max,k+1}$	…	$BH_{max,N-1}$	$BH_{max,N}$
			$BH_{avg,1}$	$BH_{avg,2}$	…	$BH_{avg,k-1}$	$BH_{avg,k}$	$BH_{avg,k+1}$	…	$BH_{avg,N-1}$	$BH_{avg,N}$

Figure 6. BL and BH, BL_{avg}, BH_{avg}, BL_{max}, and BH_{max}.

Finally, the pairs BL_k, $BH_{max,k}$ as well as BL_k, $BH_{avg,k}$ are represented in a scatterplot to identify the irregularities of the profile. For example, the Figure 7 shows the curves based on SL_{max} equal to 12 m and referring to a true measured profile.

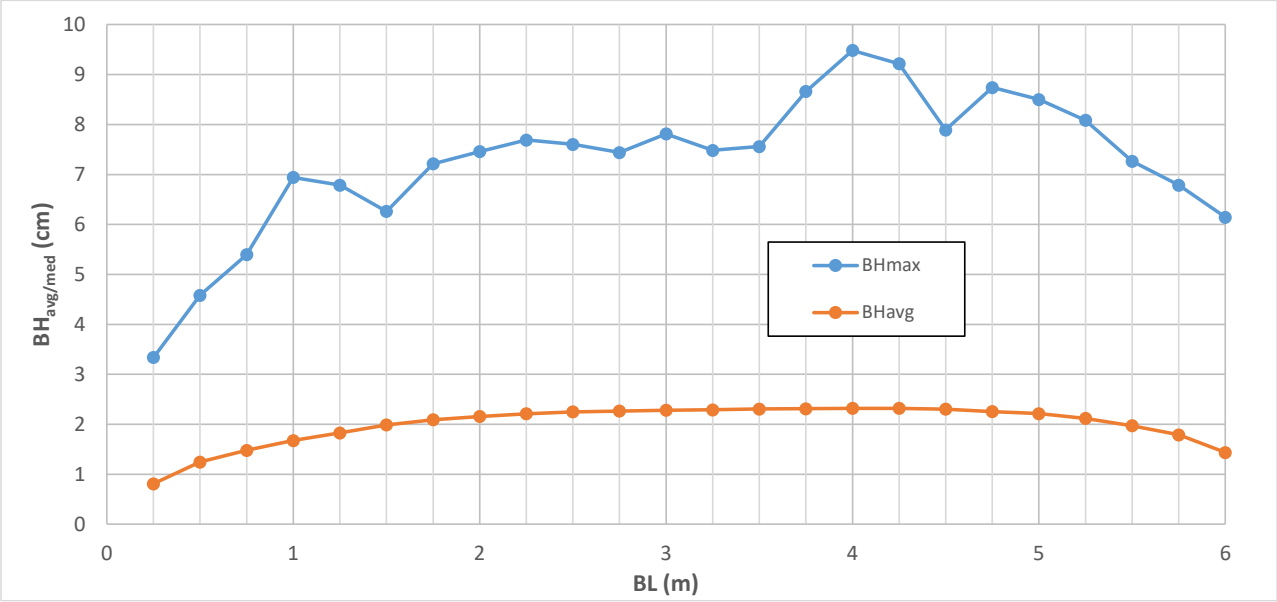

Figure 7. Example of BH curves calculated with SL_{max} = 12 m.

In order to evaluate the effect of irregularities on wavelengths comparable to the dimensions of the vehicle, the proper choice of SL_{max} is in accordance with the expected traffic. In the event of roads travelled by vehicles with very different pitches, it is better to draw BH curves considering SL_{max} according to the vehicle pitches.

Therefore, in this paper, the authors provide a reference length SL_{max} for three typical vehicles in the urban environment (Figure 8):

- Bike SL_{max} = 1 m (BL_{max} = 0.5 m);
- Automobile SL_{max} = 3 m (BL_{max} = 1.5 m);
- Bus SL_{max} = 6 m (BL_{max} = 3 m).

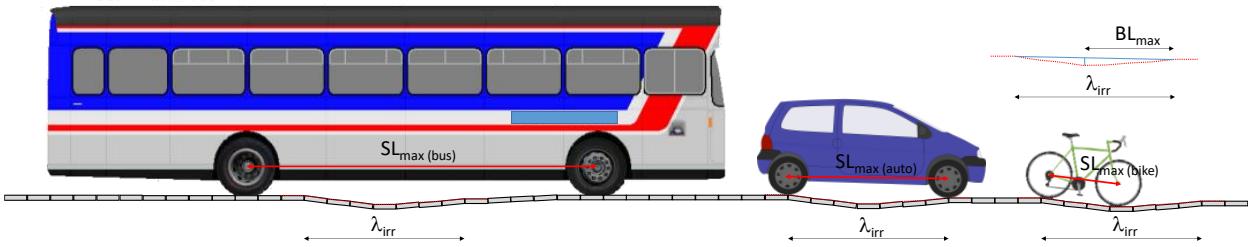

Figure 8. The effect of irregularities on wavelengths comparable to the dimensions of the vehicles.

In regards to less than 0.5 m BL values, it was appropriate to refer to the value of BH determined with SL_{max} = 1 m because they were representative of the real travel conditions for the bike category. On the other hand, BL values between 0.5 and 1.5 m were properly obtained considering SL_{max} = 3 m in order to identify the wavelengths that affected the riding conditions of automobiles. For buses, BL values between 1.5 and 3.0 m were considered. The envelope of all the BH curves enabled us to synthesize the geometric analysis of the examined pavement profile. The final BH curves were composed of branches from the BH curves obtained for each modelled vehicle (E_{max} and E_{avg} from BH_{max} and BH_{avg} curves, respectively), having regard to the discussed BL ranges. Figure 9 represents E_{avg} (green solid curve) derived from bike BH_{avg} (dotted blue curve), automobile BH_{avg} (dotted black curve) and bus BH_{avg} (dotted red curve), and E_{max} (yellow solid curve) derived from bike BH_{max} (dashed blue curve), automobile BH_{max} (dashed black curve) and bus BH_{max} (dashed red curve).

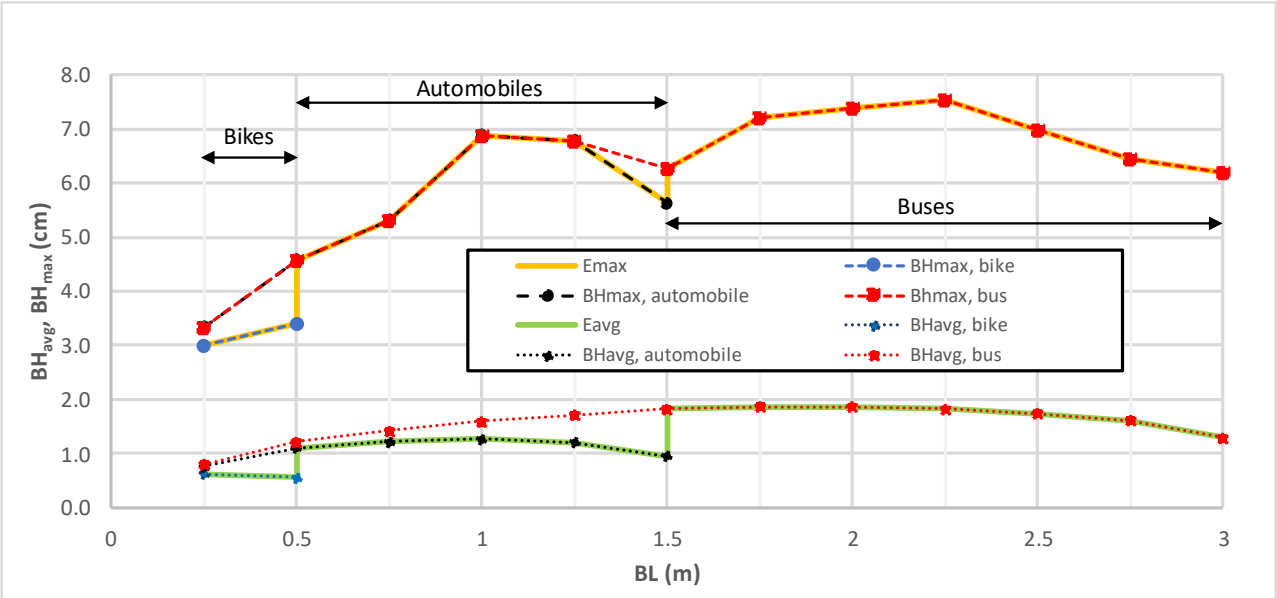

Figure 9. Example of BH envelope curves.

According to Figure 9, the envelope curves are not continuous for BL values equal to 0.5 m and 1.5 m corresponding to the vehicle category change that occurs (bike/automobile and automobile/bus).

3. Conclusions

In recent years, the interest in stone pavements has grown because of their historic heritage and physical properties, as well as environmental issues. Due to their resistance, stone pavers generally require limited and timely interventions to restore defects that cause unsafe or uncomfortable journeys. However, no standard monitoring methods or criteria for evaluating stone pavements are available in the scientific literature to assess

their functional performance and implement a pavement management system. The current lack of an effective assessing method for this type of pavement has consequences in terms of road safety and cost management.

Several methods allow for measuring and assessing irregularities of asphalt and concrete pavements; these methods provide different approaches based on the geometric profiles detected. In particular, in this paper, four methods have been investigated to describe pavement unevenness: the International Roughness Index, the surface profile classification according to ISO 8608, the vehicle mechanical model to evaluate the comfort index according to ISO 2631-1 (a_{wz}), and SASP, which is able to evaluate the effect of localized irregularities. This paper provides a critical analysis of both traditional and innovative methods of monitoring stone pavements by measuring and assessing their irregularities in order to then implement a pavement management system. IRI is defined for continuous pavements and does not provide thresholds valid for modular pavements; the classification according to ISO 8608 allow comparison between pavements but it does not support the maintenance decisions of road managers; the analysis according to ISO 2631-1 uses vehicle mechanical models (in this study, bikes, automobiles, and buses) to investigate riding conditions, but it does not allow identification of single defects to be restored.

This study focuses on the definition of SASP to overcome these aforementioned limitations. SASP allows for the identification of the most severe irregularities (for example with respect to the running conditions of the vehicles) and also their position. It will be implemented in the second part of the paper, and threshold curves will be proposed for different vehicles and operating conditions. In particular, several urban profiles have been investigated to evaluate the effects of localized irregularities taking into account different urban users (bike, automobile, and bus). The results, presented in part II, allowed the authors to propose four classes to describe geometric and comfort stone pavement conditions that consider also their effects on vulnerable road users.

Author Contributions: Conceptualization, G.L. and S.B.; methodology, G.L. and G.C.; software, G.L. and S.B.; validation, P.D.M., A.D. and L.M.; formal analysis, G.L.; investigation, G.L. and S.B.; resources, A.D. and P.D.M.; data curation, G.C., P.D.M. and L.M.; writing—original draft preparation, G.L.; writing—review and editing, G.L., P.D.M. and S.B.; visualization, L.M.; supervision, A.D. and G.C.; project administration, G.L. and P.D.M.; funding acquisition, A.D. All authors have read and agreed to the published version of the manuscript.

Funding: This research was developed within the PRIN 2017 "Stone pavements. History, conservation, valorisation and design" (20174JW7ZL) financed by the Ministry of Education, University and Research (MIUR) of the Italian Government and within the grant number RM120172B05C0B39, title "Urban pavement monitoring system using car and bike/scooter sharing vehicles" financed by Sapienza, University of Rome.

Institutional Review Board Statement: Not applicable.

Informed Consent Statement: Not applicable.

Data Availability Statement: The data presented in this study are available on request from the corresponding author.

Acknowledgments: The Authors thank Cristiano Fustaino and we acknowledge his work. He surveyed and collected the measurements on the pavements, and he applied the software implemented by the Authors for the irregularities assessment.

Conflicts of Interest: The authors declare no conflict of interest. The funders had no role in the design of the study; in the collection, analyses, or interpretation of data; in the writing of the manuscript; or in the decision to publish the results.

Appendix A

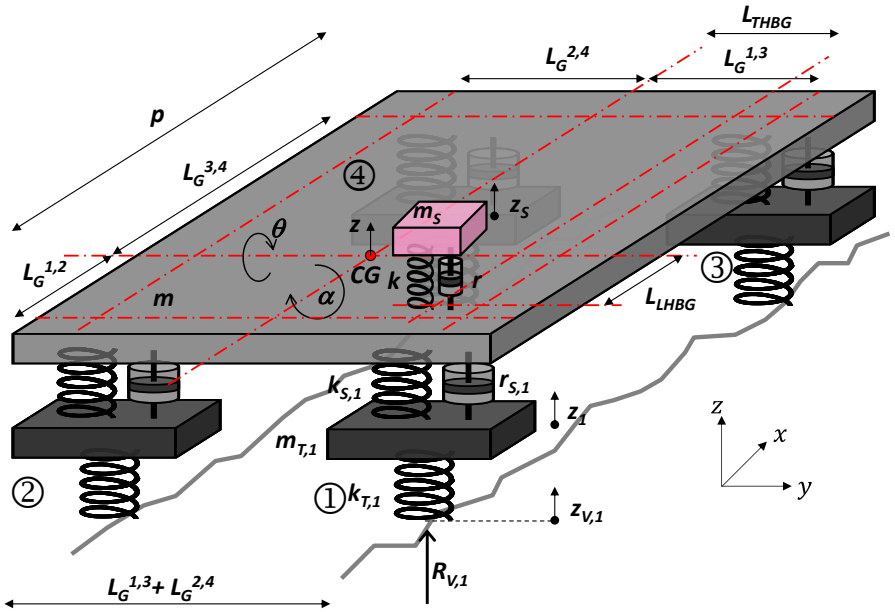

Figure A1. 8 dof mechanical automobile/bus model.

Elements of the Matrices

$$A_{1,1} = 0\ A_{1,2} = 1\ A_{1,3-16} = 0$$

$$A_{2,1} = -(k_{s1} + k_{s2} + k_{s3} + k_{s4} + k)/m\ A_{2,2} = -(c_{s1} + c_{s2} + c_{s3} + c_{s4} + c)/m\ A_{2,3} = k_{s1}/m\ A_{2,4} = c_{s1}/m$$

$$A_{2,5} = k_{s2}/m\ A_{2,6} = c_{s2}/m\ A_{2,7} = k_{s3}/m\ A_{2,8} = c_{s3}/m\ A_{2,9} = k_{s4}/m\ A_{2,10} = c_{s4}/m$$

$$A_{2,11} = (-k_{s1}\cdot L_G^{1,2} - k_{s2}\cdot L_G^{1,2} + k_{s3}\cdot L_G^{3,4} + k_{s4}\cdot L_G^{3,4} - k\cdot L_L^{S,G})/m$$

$$A_{2,12} = (-c_{s1}\cdot L_G^{1,2} - c_{s2}\cdot L_G^{1,2} + c_{s3}\cdot L_G^{3,4} + c_{s4}\cdot L_G^{3,4} - c\cdot L_L^{S,G})/m$$

$$A_{2,13} = (k_{s1}\cdot L_G^{1,3} - k_{s2}\cdot L_G^{2,4} + k_{s3}\cdot L_G^{1,3} - k_{s4}\cdot L_G^{2,4} + k\cdot L_T^{S,G})/m$$

$$A_{2,14} = (c_{s1}\cdot L_G^{1,3} - c_{s2}\cdot L_G^{2,4} + c_{s3}\cdot L_G^{1,3} - c_{s4}\cdot L_G^{2,4} + k\cdot L_T^{S,G})/m\ A_{2,15} = k/m\ A_{2,16} = c/m$$

$$A_{3,1-3} = 0\ A_{3,4} = 1\ A_{3,5-16} = 0$$

$$A_{4,1} = k_{s1}/m_{t1}\ A_{4,2} = c_{s1}/m_t\ A_{4,3} = -(k_{t1} + k_{s1})/m_{t1}\ A_{4,4} = -c_{s1}/m_{t1}\ A_{4,5-10} = 0$$

$$A_{4,11} = k_{s1}\cdot L_G^{1,2}/m_{t1}\ A_{4,12} = c_{s1}\cdot L_G^{1,2}/m_{t1}\ A_{4,13} = -k_{s1}\cdot L_G^{1,3}/m_{t1}\ A_{4,14} = -c_{s1}\cdot L_G^{1,3}/m_{t1}\ A_{4,15-16} = 0$$

$$A_{5,1-5} = 0\ A_{5,6} = 1\ A_{5,7-16} = 0$$

$$A_{6,1} = k_{s2}/m_{t2}\ A_{6,2} = c_{s2}/m_{t2}\ A_{6,3-4} = 0\ A_{6,5} = -(k_{t2} + k_{s2})/m_{t2}\ A_{6,6} = -c_{s2}/m_{t2}\ A_{6,7-10} = 0$$

$$A_{6,11} = k_{s2} \cdot L_G^{1,2}/m_{t2}\ A_{6,12} = c_{s2} \cdot L_G^{1,2}/m_{t2}\ A_{6,13} = k_{s2} \cdot L_G^{2,4}/m_{t2}\ A_{6,14} = c_{s2} \cdot L_G^{2,4}/m_{t2}\ A_{6,15-16} = 0$$

$$A_{7,1-7} = 0\ A_{7,8} = 1\ A_{7,9-16} = 0$$

$$A_{8,1} = k_{s3}/m_{t3}\ A_{8,2} = c_{s3}/m_{t3}\ A_{8,3-6} = 0\ A_{8,7} = -(k_{t3} + k_{s3})/m_{t3}\ A_{8,8} = -c_{s3}/m_{t3}\ A_{8,9-10} = 0$$

$$A_{8,11} = -k_{s3} \cdot L_G^{3,4}/m_{t3}\ A_{8,12} = -c_{s3} \cdot L_G^{3,4}/m_{t3}\ A_{8,13} = -k_{s3} \cdot L_G^{1,3}/m_{t3}\ A_{8,14} = -c_{s3} \cdot L_G^{1,3}/m_{t3}\ A_{8,15-16} = 0$$

$$A_{9,1-9} = 0\ A_{9,10} = 1\ A_{9,11-16} = 0$$

$$A_{10,1} = k_{s4}/m_{t4}\ A_{10,2} = c_{s4}/m_{t4}\ A_{10,3-8} = 0\ A_{10,9} = -(k_{t4} + k_{s4})/m_{t4}\ A_{10,10} = -c_{s4}/m_{t4}$$

$$A_{10,11} = -k_{s4} \cdot L_G^{3,4}/m_{t4}\ A_{10,12} = -c_{s4} \cdot L_G^{3,4}/m_{t4}\ A_{10,13} = k_{s4} \cdot L_G^{2,4}/m_{t4}\ A_{10,14} = c_{s4} \cdot L_G^{2,4}/m_{t4}\ A_{10,15-16} = 0$$

$$A_{11,1-11} = 0\ A_{11,12} = 1\ A_{11,13-16} = 0$$

$$A_{12,1} = (-k_{s1} \cdot L_G^{1,2} - k_{s2} \cdot L_G^{1,2} + k_{s3} \cdot L_G^{3,4} + k_{s4} \cdot L_G^{3,4} - k \cdot L_L^{S,G})/J_\theta$$

$$A_{12,2} = (-c_{s1} \cdot L_G^{1,2} - c_{s2} \cdot L_G^{1,2} + c_{s3} \cdot L_G^{3,4} + c_{s4} \cdot L_G^{3,4} - c \cdot L_L^{S,G})/J_\theta\ A_{12,3} = k_{s1} \cdot L_G^{1,2}/J_\theta\ A_{12,4} = c_{s1} \cdot L_G^{1,2}/J_\theta$$

$$A_{12,5} = k_{s2} \cdot L_G^{1,2}/J_\theta\ A_{12,6} = c_{s2} \cdot L_G^{1,2}/J_\theta\ A_{12,7} = k_{s3} \cdot L_G^{3,4}/J_\theta\ A_{12,8} = c_{s3} \cdot L_G^{3,4}/J_\theta\ A_{12,9} = k_{s4} \cdot L_G^{3,4}/J_\theta$$

$$A_{12,10} = c_{s4} \cdot L_G^{3,4}/J_\theta\ A_{12,11} = -(k_{s1} \cdot L_G^{1,2^2} + k_{s2} \cdot L_G^{1,2^2} + k_{s3} \cdot L_G^{3,4^2} + k_{s4} \cdot L_G^{3,4^2} + k \cdot L_L^{S,G^2})/J_\theta$$

$$A_{12,12} = -(c_{s1} \cdot L_G^{1,2^2} + c_{s2} \cdot L_G^{1,2^2} + c_{s3} \cdot L_G^{3,4^2} + c_{s4} \cdot L_G^{3,4^2} + c \cdot L_L^{S,G^2})/J_\theta$$

$$A_{12,13} = (k_{s1} \cdot L_G^{1,2} \cdot L_G^{1,3} - k_{s2} \cdot L_G^{1,2} \cdot L_G^{2,4} - k_{s3} \cdot L_G^{1,3} \cdot L_G^{3,4} + k_{s4} \cdot L_G^{2,4} \cdot L_G^{3,4} + k \cdot L_L^{S,G} \cdot L_T^{S,G})/J_\theta$$

$$A_{12,14} = (c_{s1} \cdot L_G^{1,2} \cdot L_G^{1,3} - c_{s2} \cdot L_G^{1,2} \cdot L_G^{2,4} - c_{s3} \cdot L_G^{1,3} \cdot L_G^{3,4} + c_{s4} \cdot L_G^{2,4} \cdot L_G^{3,4} + c \cdot L_L^{S,G} \cdot L_T^{S,G})/J_\theta\ A_{12,15} = k \cdot L_L^{S,G}/J_\theta$$

$$A_{12,16} = c \cdot L_L^{S,G}/J_\theta$$

$$A_{13,1-13} = 0\ A_{13,14} = 1\ A_{13,15-16} = 0$$

$$A_{14,1} = (k_{s1} \cdot L_G^{1,3} - k_{s2} \cdot L_G^{2,4} + k_{s3} \cdot L_G^{1,3} - k_{s4} \cdot L_G^{2,4} - k \cdot L_T^{S,G})/J_\alpha$$

$$A_{14,2} = (c_{s1} \cdot L_G^{1,3} - c_{s2} \cdot L_G^{2,4} + c_{s3} \cdot L_G^{1,3} - c_{s4} \cdot L_G^{2,4} - c \cdot L_T^{S,G})/J_\alpha\ A_{14,3} = -k_{s1} \cdot L_G^{1,3}/J_\alpha\ A_{14,4} = -c_{s1} \cdot L_G^{1,3}/J_\alpha$$

$$A_{14,5} = k_{s2} \cdot L_G^{2,4}/J_\alpha\ A_{14,6} = c_{s2} \cdot L_G^{2,4}/J_\alpha\ A_{14,7} = -k_{s3} \cdot L_G^{1,3}/J_\alpha\ A_{14,8} = -c_{s3} \cdot L_G^{1,3}/J_\alpha\ A_{14,9} = k_{s4} \cdot L_G^{2,4}/J_\alpha$$

$$A_{14,10} = c_{s4} \cdot L_G^{2,4}/J_\alpha\ A_{14,11} = (k_{s1} \cdot L_G^{1,2} \cdot L_G^{1,3} - k_{s2} \cdot L_G^{1,2} \cdot L_G^{2,4} - k_{s3} \cdot L_G^{1,3} \cdot L_G^{3,4} + k_{s4} \cdot L_G^{2,4} \cdot L_G^{3,4} + k \cdot L_L^{S,G} \cdot L_T^{S,G})/J_\alpha$$

$$A_{14,12} = (c_{s1} \cdot L_G^{1,2} \cdot L_G^{1,3} - c_{s2} \cdot L_G^{1,2} \cdot L_G^{2,4} - c_{s3} \cdot L_G^{1,3} \cdot L_G^{3,4} + c_{s4} \cdot L_G^{2,4} \cdot L_G^{3,4} + c \cdot L_L^{S,G} \cdot L_T^{S,G})/J_\alpha$$

$$A_{14,13} = -(k_{s1}\cdot L_G^{1,3^2} + k_{s2}\cdot L_G^{2,4^2} + k_{s3}\cdot L_G^{1,3^2} + k_{s4}\cdot L_G^{2,4^2} + k\cdot L_T^{S,G^2})/J_\alpha$$

$$A_{14,14} = -(c_{s1}\cdot L_G^{1,3^2} + c_{s2}\cdot L_G^{2,4^2} + c_{s3}\cdot L_G^{1,3^2} + c_{s4}\cdot L_G^{2,4^2} + c\cdot L_T^{S,G^2})/J_\alpha \; A_{14,15} = -k\cdot L_T^{S,G}/J_\alpha \; A_{14,16} = c\cdot L_T^{S,G}/J_\alpha$$

$$A_{15,1-15} = 0 \; A_{15,16} = 1$$

$$A_{16,1} = k/m_s \; A_{16,2} = c/m_s \; A_{16,3-10} = 0 \; A_{16,11} = k\cdot L_L^{S,G}/m_s \; A_{16,12} = c\cdot L_L^{S,G}/m_s \; A_{16,13} = -k\cdot L_T^{S,G}/m_s$$

$$A_{16,14} = -c\cdot L_T^{S,G}/m_s \; A_{16,15} = -k/m_s \; A_{16,16} = -c/m_s$$

$$B_{1-3,1-4} = 0 \; B_{4,1} = k_{t1}/m_{t1} \; B_{4,2-4} = 0 \; B_{5,1-4} = 0 \; B_{6,1} = 0 \; B_{6,2} = k_{t2}/m_{t2} \; B_{6,3-4} = 0 \; B_{7,1-4} = 0$$

$$B_{8,1-2} = 0 \; B_{8,3} = k_{t3}/m_{t3} \; B_{8,4} = 0 \; B_{9,1-4} = 0 \; B_{10,1-3} = 0 \; B_{10,4} = k_{t4}/m_{t4}\cdot B_{11-16,1-4} = 0$$

$$C_{1,1-2} = 0 \; C_{1,3} = k_{t1} \; C_{1,4-16} = 0 \; C_{2,1-4} = 0 \; C_{2,5} = k_{t2} \; C_{2,6-16} = 0 \; C_{3,1-6} = 0 \; C_{3,7} = k_{t3} \; C_{3,8-16} = 0$$

$$C_{4,1-8} = 0 \; C_{4,9} = k_{t4} \; C_{4,10-16} = 0$$

$$D_{1,1} = -k_{t1} \; D_{1,2-4} = 0 \;\; D_{2,1} = 0 \;\; D_{2,2} = -k_{t2} \; D_{2,3-4} = 0 \;\; D_{3,1-2} = 0 \;\; D_{3,3} = -k_{t3} \; D_{3,4} = 0 \; D_{4,1-3} = 0$$

$$D_{4,4} = -k_{t4}$$

$$a_s(t) = \frac{k\cdot[z(t) - z_s(t)] - r\cdot\left[\dot{z}_s(t) - \dot{z}(t)\right] + k\cdot\left[L_L^{S,G}\cdot\theta(t) - L_T^{S,G}\cdot\alpha(t)\right] - r\left[L_T^{S,G}\cdot\dot{\alpha}(t) - L_L^{S,G}\cdot\dot{\theta}(t)\right]}{m_s}$$

Table A1. Automobile Data.

Symbol	Value	Unit	Description
m_s	100	kg	Driver body mass
m	1300	kg	Sprung vehicle mass
$m_{t,1}$	40	kg	Tire front/left–unsprung mass 1
$m_{t,2}$	40	kg	Tire front/right–unsprung mass 2
$m_{t,3}$	35	kg	Tire rear/left–unsprung mass 3
$m_{t,4}$	35	kg	Tire rear/right–unsprung mass 4
J_θ	2700	kg m^2	Body (automobile) sprung mass pitch moment of inertia
J_α	400	kg m^2	Body (automobile) sprung mass roll moment of inertia
p	2.59	m	Automobile wheelbase
$L_G^{1,2}$	1.0	m	Distance between front-axle/CG
$L_G^{3,4}$	1.59	m	Distance between rear-axle/CG
$L_G^{1,3}$	0.8	m	Axle semi width (left)
$L_G^{2,4}$	0.8	m	Axle semi width (right)

Table A1. *Cont.*

Symbol	Value	Unit	Description
$L_L^{S,G}$	0.2	m	Longitudinal distance between seat/CG
$L_T^{S,G}$	0.4	m	Transversal distance between seat/CG
$k_{s,1}$	38,889	N/m	Spring constant suspension front/left (1)
$k_{s,2}$	38,889	N/m	Spring constant suspension front/right (2)
$k_{s,3}$	35,000	N/m	Spring constant suspension rear/left (3)
$k_{s,4}$	35,000	N/m	Spring constant suspension rear/right (4)
$k_{t,1}$	200,000	N/m	Spring constant tire front/left (1)
$k_{t,2}$	200,000	N/m	Spring constant tire front/right (2)
$k_{t,3}$	200,000	N/m	Spring constant tire rear/left (3)
$k_{t,4}$	200,000	N/m	Spring constant tire rear/right (4)
k	87,464	N/m	Spring constant seat
$c_{s,1}$	1400	N s/m	Damping constant suspension front/left (1)
$c_{s,2}$	1400	N s/m	Damping constant suspension front/right (2)
$c_{s,3}$	1400	N s/m	Damping constant suspension rear/left (3)
$c_{s,4}$	1400	N s/m	Damping constant suspension rear/right (4)
c	3000	N s/m	Damping constant seat driver
z	var	m	Body vertical motion coordinate (1-dof)
z_1	var	m	Front/left wheel vertical motion coordinate (2-dof)
z_2	var	m	Front/right wheel vertical motion coordinate (3-dof)
z_3	var	m	Rear/left wheel vertical motion coordinate (4-dof)
z_4	var	m	Rear/right wheel vertical motion coordinate (5-dof)
z_s	var	m	Seat vertical motion coordinate (6-dof)
α	var	rad	Body roll motion coordinate (7-dof)
θ	var	rad	Body pitch motion coordinate (8-dof)
$z_{v,1}$	var	m	Road profile elevation–front/left
$z_{v,2}$	var	m	Road profile elevation–front/right
$z_{v,3}$	var	m	Road profile elevation–rear/left
$z_{v,4}$	var	m	Road profile elevation–rear/right

Table A2. Bus Data.

Symbol	Value	Unit	Description
m_s	100	kg	Driver body mass
m	15,890	kg	Sprung vehicle mass
$m_{t,1}$	373	kg	Tire front/left–unsprung mass 1
$m_{t,2}$	373	kg	Tire front/right–unsprung mass 2
$m_{t,3}$	678	kg	Tire rear/left–unsprung mass 3
$m_{t,4}$	678	kg	Tire rear/right–unsprung mass 4
J_θ	150,000	kg m^2	Body (automobile) sprung mass pitch moment of inertia
J_α	13,000	kg m^2	Body (automobile) sprung mass roll moment of inertia

Table A2. *Cont.*

Symbol	Value	Unit	Description
p	5.65	m	Bus wheelbase
$L_G^{1,2}$	3.61	m	Distance between front-axle/CG
$L_G^{3,4}$	2.04	m	Distance between rear-axle/CG
$L_G^{1,3}$	1.0	m	Axle semi width (left)
$L_G^{2,4}$	1.0	m	Axle semi width (right)
$L_L^{S,G}$	0.8	m	Longitudinal distance between seat/CG
$L_T^{S,G}$	0.5	m	Transversal distance between seat/CG
$k_{s,1}$	175,000	N/m	Spring constant suspension front/left (1)
$k_{s,2}$	175,000	N/m	Spring constant suspension front/right (2)
$k_{s,3}$	408,650	N/m	Spring constant suspension rear/left (3)
$k_{s,4}$	408,650	N/m	Spring constant suspension rear/right (4)
$k_{t,1}$	1,000,000	N/m	Spring constant tire front/left (1)
$k_{t,2}$	1,000,000	N/m	Spring constant tire front/right (2)
$k_{t,3}$	2,000,000	N/m	Spring constant tire rear/left (3)
$k_{t,4}$	2,000,000	N/m	Spring constant tire rear/right (4)
k	40,000	N/m	Spring constant seat
$c_{s,1}$	40,000	N s/m	Damping constant suspension front/left (1)
$c_{s,2}$	40,000	N s/m	Damping constant suspension front/right (2)
$c_{s,3}$	45,973	N s/m	Damping constant suspension rear/left (3)
$c_{s,4}$	45,973	N s/m	Damping constant suspension rear/right (4)
c	220	N s/m	Damping constant seat driver
z	var	m	Body vertical motion coordinate (1-dof)
z_1	var	m	Front/left wheel vertical motion coordinate (2-dof)
z_2	var	m	Front/right wheel vertical motion coordinate (3-dof)
z_3	var	m	Rear/left wheel vertical motion coordinate (4-dof)
z_4	var	m	Rear/right wheel vertical motion coordinate (5-dof)
z_s	var	m	Seat vertical motion coordinate (6-dof)
α	var	rad	Body roll motion coordinate (7-dof)
θ	var	rad	Body pitch motion coordinate (8-dof)
$z_{v,1}$	var	m	Road profile elevation–front/left
$z_{v,2}$	var	m	Road profile elevation–front/right
$z_{v,3}$	var	m	Road profile elevation–rear/left
$z_{v,4}$	var	m	Road profile elevation–rear/right

References

1. Bruno, S.; Vita, L.; Loprencipe, G. Development of a GIS-Based Methodology for the Management of Stone Pavements Using Low-Cost Sensors. *Sensors* **2022**, *22*, 6560. [CrossRef] [PubMed]
2. International Organization for Standardization (ISO) Characterization of Pavement Texture by Use of Surface Profiles-Part 2: Terminology and Basic Requirements Related to Pavement Texture Profile Analysis. Available online: https://www.iso.org/standard/25638.html (accessed on 20 June 2022).
3. Di Mascio, P.; Moretti, L.; Capannolo, A. Concrete Block Pavements in Urban and Local Roads: Analysis of Stress-Strain Condition and Proposal for a Catalogue. *J. Traffic Transp. Eng.* **2019**, *6*, 557–566. [CrossRef]

4. Bonin, G.; Cantisani, G.; Loprencipe, G.; Ranzo, A. Dynamic effects in concrete airport pavement joints. [Effetti dinamici nei giunti delle pavimentazioni aeroportuali in calcestruzzo]. *Ind. Ital. Cem.* **2007**, *77*, 590–607.
5. Zoccali, P.; Moretti, L.; Di Mascio, P.; Loprencipe, G.; D'Andrea, A.; Bonin, G.; Teltayev, B.; Caro, S. Analysis of natural stone block pavements in urban shared areas. *Case Stud. Constr. Mater.* **2018**, *8*, 498–506. [CrossRef]
6. Moretti, L.; Cantisani, G.; Carpiceci, M.; D'andrea, A.; Del Serrone, G.; Di Mascio, P.; Peluso, P.; Loprencipe, G. Investigation of Parking Lot Pavements to Counteract Urban Heat Islands. *Sustainability* **2022**, *14*, 7273. [CrossRef]
7. Hu, J.; Gao, X.; Wang, R.; Sun, S. Research on Comfort and Safety Threshold of Pavement Roughness. *Transp. Res. Rec.* **2017**, *2641*, 149–155. [CrossRef]
8. Sun, L.; Chen, L.; Yin, Y.; Tian, Y.; Zhang, X. Risk Assessment of Rollover and Skidding due to Pavement Roughness and Differential Settlement for Enhancing Transportation Safety. *J. Adv. Transp.* **2021**, *2021*, 7244283. [CrossRef]
9. Organisation for Economic Co-Operation and Development (OECD); Forum, (ITF) International Transport. *Improving Safety for Motorcycle, Scooter and Moped Riders*; Organisation de Cooperation et de Developpement Economiques-OCDE: Paris, France, 2015; Volume 212.
10. Bella, F.; Calvi, A.; D'Amico, F. Impact of Pavement Defects on Motorcycles' Road Safety. *Procedia—Soc. Behav. Sci.* **2012**, *53*, 942–951. [CrossRef]
11. Abdul Manan, M.M.; Várhelyi, A.; Çelik, A.K.; Hashim, H.H. Road characteristics and environment factors associated with motorcycle fatal crashes in Malaysia. *IATSS Res.* **2018**, *42*, 207–220. [CrossRef]
12. D'Amico, F.; Calvi, A.; Bianchini Ciampoli, L.; Tosti, F.; Brancadoro, M.G. Evaluation of the impact of pavement degradation on driving comfort and safety using a dynamic simulation model. *Adv. Transp. Stud.* **2018**, *1*, 109–120.
13. Cuomo, V. The Influence of Roughness, Evenness and Road Geometry on Wheel-Road Interaction by Means of a Numerical Simulation Procedure. In Proceedings of the III SIIV International Conference, Bari, Italy, 22–24 September 2005.
14. Rome Capital | Institutional Site | Piano Sanpietrini on the Streets of Rome. Available online: https://www.comune.roma.it/web/it/notizia.page?contentId=NWS330358 (accessed on 20 June 2022).
15. Strade Ammalorate, Al via IL Ripristino della Pavimentazione—Sito Ufficio Stampa Comune di Modena. Available online: https://www.comune.modena.it/salastampa/archivio-comunicati-stampa/2020/9/strade-ammalorate-al-via-il-ripristino-della-pavimentazione (accessed on 20 June 2022).
16. Sandberg, U.; Bendtsen, H.; Thomsen, S.N.; Kragh, J.; Kalman, B.; Kokot, D. *Possibilities to Reduce Tyre/Road Noise Emission on Paving Stones and Other Block Surfaces*; European Commission DG Research: Bruxelles, Belgium, 2007.
17. Cantisani, G.; Fascinelli, G.; Loprencipe, G. Urban Road Noise: The Contribution of Pavement Discontinuities. In Proceedings of the 2012 International Conference on Sustainable Design and Construction, Fort Worth, TX, USA, 7–9 November 2012; American Society of Civil Engineers: Reston, VA, USA; pp. 327–334. [CrossRef]
18. Bruno, S.; Del Serrone, G.; Di Mascio, P.; Loprencipe, G.; Ricci, E.; Moretti, L. Technical proposal for monitoring thermal and mechanical stresses of a runway pavement. *Sensors* **2021**, *21*, 6797. [CrossRef] [PubMed]
19. Kulkarni, R.B. Dynamic Decision Model for a Pavement Management System. *Transp. Res. Rec.* **1984**, *997*, 11–18.
20. Zoccali, P.; Loprencipe, G.; Galoni, A. Sampietrini Stone Pavements: Distress Analysis Using Pavement Condition Index Method. *Appl. Sci.* **2017**, *7*, 669. [CrossRef]
21. Garilli, E.; Autelitano, F.; Freddi, F.; Giuliani, F. Urban pedestrian stone pavements: Measuring functional and safety requirements. *Int. J. Pavement Eng.* **2022**, *23*, 4748–4759. [CrossRef]
22. Qiao, J.Y.; Du, R.; Labi, S.; Fricker, J.D.; Sinha, K.C. Policy implications of standalone timing versus holistic timing of infrastructure interventions: Findings based on pavement surface roughness. *Transp. Res. Part A Policy Pract.* **2021**, *148*, 79–99. [CrossRef]
23. Múčka, P. International Roughness Index specifications around the world. *Road Mater. Pavement Des.* **2017**, *18*, 929–965. [CrossRef]
24. Sidess, A.; Ravina, A.; Oged, E. A model for predicting the deterioration of the international roughness index. *Int. J. Pavement Eng.* **2022**, *23*, 1393–1403. [CrossRef]
25. Corley-Lay, J. Pavement Performance Measures How States See Good, Fair, and Poor. *Transp. Res. Rec.* **2014**, *2431*, 1–5. [CrossRef]
26. Bennett, C. Sectioning of road data for pavement management. In Proceedings of the 6th International Conference on Managing Pavements: The Lessons, The Challenges, The Way AheadQueensland Department of Main RoadsARRBFRH GroupExor CorporationPavement Management ServicesFederal Highway AdministrationWorld HighwaysGHDBrisbane City CouncilTasmania Department of Infrastructure, Energy and ResourcesAustralian Road Federation (ARF) HansenCooperative Research Centre for Construction Innovation, Brisbane Queensland, Australia, 19–24 October 2004.
27. Papagiannakis, A.; Woodrooffe, J. Suitability of Alternative Pavement Roughness Statistics to Describe Dynamic Axle Loads of Heavy Vehicles. In Proceedings of the 2nd International Symposium on Heavy Vehicle Weights and Dimensions, Kelowna, BC, Canada, 18–22 June 1989.
28. Kırbaş, U. Determination of ride comfort thresholds based on international roughness index for asphalt concrete pavements. *Int. J. Pavement Eng.* **2021**, 1–13. [CrossRef]
29. Múčka, P. Road Roughness Limit Values Based on Measured Vehicle Vibration. *J. Infrastruct. Syst.* **2017**, *23*, 04016029. [CrossRef]
30. Nguyen, T.; Lechner, B.; Wong, Y.D.; Tan, J.Y. Bus Ride Index—A refined approach to evaluating road surface irregularities. *Road Mater. Pavement Des.* **2021**, *22*, 423–443. [CrossRef]
31. Múčka, P. Vibration Dose Value in Passenger Car and Road Roughness. *J. Transp. Eng. Part B Pavements* **2020**, *146*, 04020064. [CrossRef]

32. Loprencipe, G.; Zoccali, P.; Cantisani, G. Effects of vehicular speed on the assessment of pavement road roughness. *Appl. Sci.* **2019**, *9*, 1783. [CrossRef]
33. Cantisani, G.; Loprencipe, G. Road Roughness and Whole Body Vibration: Evaluation Tools and Comfort Limits. *J. Transp. Eng.* **2010**, *136*, 818–826. [CrossRef]
34. Yu, J.; Chou, E.Y.J.; Yau, J.-T. Development of Speed-Related Ride Quality Thresholds Using International Roughness Index. *Transp. Res. Rec. J. Transp. Res. Board* **2006**, *1974*, 47–53. [CrossRef]
35. Múčka, P. International Roughness Index Thresholds Based on Whole-Body Vibration in Passenger Cars. *Transp. Res. Rec.* **2020**, *2675*, 305–320. [CrossRef]
36. La Torre, F. Criteri e valutazione delle irregolarità stradali localizzate. In *Proceedings of the Adeguamento Funzionale e Manutenzione delle Infrastrutture Viarie*; SIIV: Milano, Italy, 1998; pp. 224–230. (In Italian)
37. La Torre, F.; Ballerini, L.; Di Volo, N. Correlation between longitudinal roughness and user perception in urban areas. *Transp. Res. Rec.* **2002**, *1806*, 131–139. [CrossRef]
38. *ISO 8608*; Mechanical Vibration—Road Surface Profiles—Reporting of Measured Data. International Organization for Standardization: Geneva, Switzerland, 2016.
39. Elson, J.M.; Bennett, J.M. Calculation of the power spectral density from surface profile data. *Appl. Opt.* **1995**, *34*, 201. [CrossRef]
40. Gandhi, P.; Adarsh, S.; Ramachandran, K.I. Performance Analysis of Half Car Suspension Model with 4 DOF using PID, LQR, FUZZY and ANFIS Controllers. *Procedia Comput. Sci.* **2017**, *115*, 2–13. [CrossRef]
41. Klockiewicz, Z.; Ślaski, G.; Spadło, M. *The Influence of the Conditions of Use and the Type of Model Used on the Vertical Dynamic Responses of a Car Suspension*; The Archives of Automotive Engineering –Archiwum Motoryzacji: Scientific Publishers of the Industrial Motorization Institute: Warsaw, Poland, 2019; Volume 85, pp. 57–82.
42. Mucka, P. Simulated Road Profiles According to ISO 8608 in Vibration Analysis. *J. Test. Eval.* **2018**, *46*, 405–418.
43. Loprencipe, G.; Zoccali, P. Use of generated artificial road profiles in road roughness evaluation. *J. Mod. Transp.* **2017**, *25*, 24–33. [CrossRef]
44. Johannesson, P.; Rychlik, I. Modelling of road profiles using roughness indicators. *Int. J. Veh. Des.* **2014**, *66*, 317–346. [CrossRef]
45. Kropac, O.; Mucka, P. Be careful when using the International Roughness Index as an indicator of road unevenness. *J. Sound Vib.* **2005**, *287*, 989–1003. [CrossRef]
46. Sirocchi, C.; Klopfenstein, L.C.; Bogliolo, A. Large-Scale Assessment of Mobile Crowdsensed Data: A Case Study. *IEEE Access* **2022**, *10*, 54681–54696. [CrossRef]
47. Loprencipe, G.; de Almeida Filho, F.G.V.; de Oliveira, R.H.; Bruno, S. Validation of a Low-Cost Pavement Monitoring Inertial-Based System for Urban Road Networks. *Sensors* **2021**, *21*, 3127. [CrossRef]
48. *ISO 2631-1*; Mechanical Vibration and Shock-Evaluation of Human Exposure to Whole-Body Vibration. International Organization for Standardization: Geneva, Switzerland, 1997.
49. FAA. *Guidelines and Procedures for Measuring Airfield Pavement Roughness*; FAA: Washington, DC, USA, 2014.
50. *ASTM E1926-08*; Standard Practice for Computing International Roughness Index of Roads from Longitudinal Profile Measurements. ASTM International: West Conshohocken, PA, USA, 2015.
51. Sayers, M.W. On the calculation of International Roughness Index from longitudinal road profile. *Transp. Res. Rec.* **1995**, *1501*, 1–12.
52. Sayers, M.W.; Gillespie, T.D.; Queiroz, C.A.V. *The International Road Roughness Experiment: Establishing Correlation and a Calibration Standard for Measurements*; The World Bank: Washington, DC, USA, 1986.
53. Goenaga, B.; Fuentes, L.; Mora, O. Evaluation of the methodologies used to generate random pavement profiles based on the power spectral density: An approach based on the international roughness index. *Ing. Investig.* **2017**, *37*, 49–57. [CrossRef]
54. Podder, P.; Zaman Khan, T.; Haque Khan, M.; Muktadir Rahman, M. Comparative Performance Analysis of Hamming, Hanning and Blackman Window. *Int. J. Comput. Appl.* **2014**, *96*, 1–7. [CrossRef]
55. Múčka, P.; Granlund, J. Is the road quality still better? *J. Transp. Eng.* **2012**, *138*, 1520–1529. [CrossRef]
56. Agostinacchio, M.; Ciampa, D.; Olita, S. The vibrations induced by surface irregularities in road pavements—A Matlab® approach. *Eur. Transp. Res. Rev.* **2014**, *6*, 267–275. [CrossRef]
57. Sidhant, V.K. Bicycle Ride Comfort Evaluation and Optimization. Master's Thesis, University of Pretoria, Pretoria, South Africa, 2019.
58. Soffarina, M.S.S. Mountain Bicycle Cycling Comfort on Different Road Surfaces. *J. Sci. Appl. Eng.* **2020**, *3*(1), 29–34. [CrossRef]
59. Gogola, M. Analysing the vibration of bicycles on various road surfaces in the city of Žilina. *Arch. Motoryz.* **2020**, *88*, 77–97. [CrossRef]
60. Huang, J.; Fournier, N.; Skabardonis, A. Bicycle level of service: Proposed updated pavement quality index. *Transp. Res. Rec.* **2021**, *2675*, 1346–1356. [CrossRef]
61. Tong, Z.; Gao, J.; Sha, A.; Hu, L.; Jiang, W.; Huang, Y. Evaluating the cycling comfort on urban roads based on cyclists' perception of vibration. *J. Clean. Prod.* **2018**, *192*, 531–541.
62. Thigpen, C.G.; Li, H.; Handy, S.L.; Harvey, J. Modeling the impact of pavement roughness on bicycle ride quality. *Transp. Res. Rec.* **2015**, *2520*, 67–77. [CrossRef]
63. Wu, R.; Louw, S.; Li, H.; Harvey, J.T.; Thigpen, C. Bicycle Vibration and Pavement Ride Quality for Cyclists. In Proceedings of the 94th Annual Meeting of the Transportation Research Board, Washington, DC, USA, 11–15 January 2015.

64. Sekulić, D.; Dedović, V.; Rusov, S.; Šalinić, S.; Obradović, A. Analysis of vibration effects on the comfort of intercity bus users by oscillatory model with ten degrees of freedom. *Appl. Math. Model.* **2013**, *37*, 8629–8644. [CrossRef]
65. Nguyen, T.; Swolana, P.; Lechner, B.; Wong, Y.D. An experimental comparison of mathematical heavy-duty city bus models to evaluate passenger ride comfort induced by road roughness. *Math. Comput. Model. Dyn. Syst.* **2021**, *27*, 203–221. [CrossRef]
66. Bay, J.S. *Fundamentals of Linear State Space Systems*, 1st ed.; McGraw-Hill Education: London, UK, 1999.
67. State-Space Model—MATLAB. Available online: https://www.mathworks.com/help/control/ref/ss.html (accessed on 25 October 2022).

Disclaimer/Publisher's Note: The statements, opinions and data contained in all publications are solely those of the individual author(s) and contributor(s) and not of MDPI and/or the editor(s). MDPI and/or the editor(s) disclaim responsibility for any injury to people or property resulting from any ideas, methods, instructions or products referred to in the content.